



Efficient Prediction of the Thermal Conductivity of Wood from Its Microscopic Morphology

El Houssaine Quenjel^(✉) and Patrick Perré

CentraleSupélec, Laboratoire de Génie Des Procédés Et Matériaux, Centre Européen de Biotechnologie Et de Bioéconomie (CEBB), Université Paris-Saclay, 3 Rue Des Rouges Terres, 51110 Pomacle, France

{el-houssaine.quenjel,patrick.perre}@centralesupelec.fr

Abstract. In this work, we combined the homogenization and finite volume methods to predict the solid fraction and the effective thermal conductivity from 3D real morphologies of wood, namely spruce and poplar. High resolution scans performed by a nano-tomograph, together with image processing are two steps of great importance to obtain the digital representation of the real morphology suitable for computation. These tools allow the generation of the 3D mesh of the thresholded sample. The stationary diffusion model is directly considered to gain in performance. Numerical results revealed that several minutes of CPU time are enough to predict the values of the thermal conductivity on the representative volumes. Compared to some of our recent works, the present methodology is not only efficient, but also more accurate.

Keywords: Thermal conductivity · Homogenization · REV · Image processing · Tomography

1 Introduction

There is an increasing interest in using insulation materials for building constructions to optimize the energy consumption [1]. Wood-based materials exhibit good features for this purpose. To understand the wood characteristics and its role in the improvement of the energy efficiency, experimental tests are often conducted. Taking advantage of tomography technology together with high performance computing, numerical prediction is also an appropriate way to estimate macroscopic properties, notably the effective conductivities [2–5].

Synchrotron facilities enable a suitable representation of the wood anatomy [6]. However, lab-equipment tomographs are nowadays able to reproduce the digital interpretation of the material structure. Scans of high resolution provide a good description of the sample with no degradation [7–12]. From the 3D scans, image processing is required for thresholding and to extract objective information such as the distribution and the partition of the phases, quantifying density, or the orientation of the cell walls.

Then, the morphology is used to proceed to homogenization, using suitable computational methods, for estimating the macroscopic properties of wood. For instance, finite

elements were investigated in [3, 13, 14] for the computation of the thermal conductivity. A finite volume approximation was carried out in [7, 15] to predict liquid diffusivity and thermal conductivity. The work established in [16] was devoted to the lattice Boltzmann meshless scheme enabling the simulation of heat and moisture diffusion in spruce and wood panels. In our recent paper [17] we developed an explicit finite volume approach allowing the prediction of the macroscopic thermal conductivity of wood. Besides the REV size constraint, working at the pore scale requires tiny time steps, which makes the convergence towards the steady state too slow. To mitigate this issue, a volume reduction strategy was also proposed following the longitudinal direction. The idea yields convenient results. However, it is based on a stronger assumption adapted to small set of materials whose phases are in parallel in the longitudinal direction.

The core point of the present contribution is to perform computations using the stationary model instead of the transient one. Its main assets are summarized as follows: (i) no reduction in the volume size is required; (ii) taking into account larger REVs is now possible (iii) spectacular gains in terms of the computational cost are reported; (iv) accuracy is ensured. Consequently, this methodology provides a better compromise to predict the macroscopic thermal conductivity efficiently and accurately.

2 Materials and Methods

2.1 Sample Preparation and Tomography

The wood samples come from well-identified boards available in our laboratory. They were dried outside before storing them in air-dry conditions. The size of the spruce and poplar species was adjusted to fit small cylindrical shapes of the order of millimeters. This was done with the help of a wood-turning machine. Such a cut is mandatory to achieve the high resolution. The diameter and the height of the cylinders were 5.64 and 3.11 mm, respectively, for spruce and poplar. All these samples are scanned at a micrometer resolution thanks to a lab X-ray nanotomograph (UltraTom by RX-solutions). The obtained 3D image of the sample is given by a heavy stack of 2D images following the longitudinal direction. We denote by (R), (T) and (L) the natural material directions, referred to as radial, tangential and longitudinal. The scanned samples are illustrated in Fig. 1. Precisely, the resolution is 3 μm for spruce and poplar.

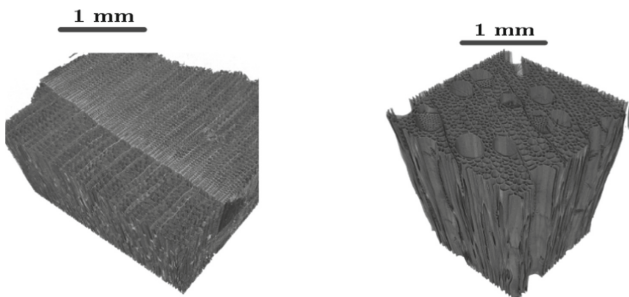


Fig. 1. Scanned sample of spruce (left) and poplar (right)

2.2 Morphology Segmentation

The image processing procedure was implemented in Python. High-resolution scans lead to large sets of data. We follow a practical idea to extract the representative elementary volume (REV) within any complex geometry. The 3D morphology is a series of 2D images. The REV is chosen by specifying its center and size. One then crops the original 3D image and applies the global segmentation methodology thanks to Otsu's automatic thresholding technique [18]. Figure 2 exhibits the results of the binary morphologies. Two phases are considered. The assigned code 255 (0) stands for the gaseous (solid) phase. The 3D mesh of the morphology is also generated at this stage. It can be seen that the cell walls are more aligned in the (R,T) section for spruce than poplar. This would have an impact on the macroscopic property.

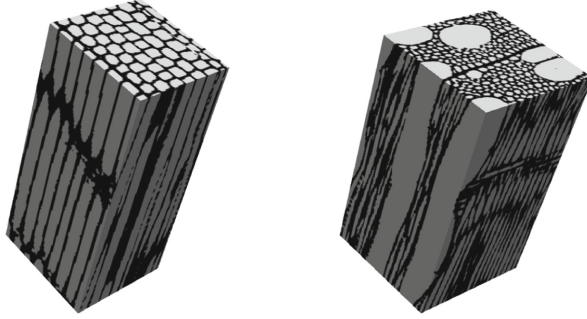


Fig. 2. Thresholded volume of spruce $101 \times 101 \times 255$ voxels (left) and thresholded volume of poplar $128 \times 128 \times 255$ voxels (right)

2.3 A Word on the Homogenization

Homogenization is a mathematical method, which consists of predicting macroscopic properties from the microscopic structure of materials [19, 20]. In this work, we focus on a stationary diffusion equation to derive the effective thermal conductivity. Let Ω be the 3D parallelepiped $\Omega = [x_0, x_m] \times [y_0, y_n] \times [z_0, z_p]$ extracted from the original morphology. Consider the problem

$$-\operatorname{div}(\alpha \nabla u) = 0, \quad (1)$$

where u accounts for temperature, and the parameter $\alpha = \lambda_0 / (\rho c_p)$ is the local thermal coefficient. The number λ_0 indicates the local thermal conductivity, ρ refers to density, and c_p informs the heat capacity. The boundary condition is given by $u^{\text{Dir}} = 1$ on the face $x = x_0$, and $u^{\text{Dir}} = 0$ on the opposite face $x = x_m$. The remaining boundary is adiabatic. In the numerical section, the factor ρc_p can be set to unity. The local thermal coefficient λ_0 is fixed to 0.5 W/m.K in the case of the solid phase and to 0.023 W/m.K for the gaseous phase. The problem (1) is solved owing to the finite volume method on the mesh of Ω . To deduce λ^l of the REV material, one evaluates the ratio of the x-flux average $\langle F_x \rangle$ to the imposed gradient $\delta u / L_x$; i.e. $\lambda^l = \langle F_x \rangle L_x / \delta u$.

2.4 The Finite Volume Approximation

Let N_Ω be the total number of degrees of freedom. The mesh $\Gamma = \{K_i, i = 1, \dots, N_\Omega\}$ is a partition of Ω with control volumes. Let x_i denote the mass center of K_i . The set of faces of K_i is denoted by E_i . Each interface $\sigma_{ij} = K_i K_j$ is shared by two volumes K_i and K_j . The latter volume is identified to an edge if the interface is located on the boundary. The unit normal to σ_{ij} from K_i to K_j is expressed by n_{ij} . The two-point approximation of the flux assumes the orthogonality condition on the mesh. This means that the line connecting x_i to x_j is orthogonal to σ_{ij} . This condition is fulfilled on hexahedral meshes in 3D generated from the morphology.

Integrating the main model (1) on K_i and using the divergence theorem yields

$$-\int_{K_i} \operatorname{div}(\alpha(x)\nabla u(x))dx = -\sum_{\sigma_{ij} \in E_i} \int_{\sigma_{ij}} \alpha(s)\nabla u(s) \cdot n_{ij}ds = 0.$$

The physical quantities are supposed constants by cells. Then, the flux is approximated in only one direction provided by the unit normal vector to the face because the other ones are orthogonal to n_{ij} . As a consequence, the numerical scheme reads

$$\sum_{\sigma_{ij} \in E_i} \tau_{ij}(u_i - u_j) = 0, \text{ for all } i = 1, \dots, N_\Omega, u_j = u_j^{\text{Dir}}, \text{ if } \sigma_{ij} \subset \partial\Omega,$$

where τ_{ij} refers to the transmissibility coefficient $\tau_{ij} = \alpha_{ij}|\sigma_{ij}|/\|x_i - x_j\|$. The coefficient α_{ij} is the harmonic average of $\alpha_i = \alpha(x_i)$ and $\alpha_j = \alpha(x_j)$.

3 Computational Results

The objective of this section is to show the ability and the efficiency of the proposed finite volume scheme to predict the macroscopic thermal conductivity. The numerical scheme is implemented in Fortran. The linear solver is based on the conjugate gradient method.

3.1 Solid Fraction

The data of the scanned samples are extremely big. Their size order are $1800 \times 1900 \times 1150$ voxels, which makes the image processing as well as the macroscopic property computations inaccessible. Then, we are led to deal with embedded volumes. For this purpose, from the initial image, we extract the REV under the form of hexahedral subset. Its center is denoted by (x_c, y_c, z_c) . The length, width and height are respectively given by $2\Delta x, 2\Delta y, 2\Delta z$. In other words, the REV writes

$$\text{REV} = [x_c - \Delta x, x_c + \Delta x] \times [y_c - \Delta y, y_c + \Delta y] \times [z_c - \Delta z, z_c + \Delta z].$$

The center of the REV is fixed to (1155, 870, 555) in the case of spruce while the center of the REV is set to (940, 940, 555) for poplar. To determine the considered dimensions, we use an increasing uniform sequence of the REV sizes containing six elements. For $l = 1, \dots, 6$ we consider $\Delta x_l = \Delta y_l = 16l, \Delta z_l = 2\Delta x_l - 1$.

Table 1. Solid fraction in terms of the REV size

REV number	Size (voxels)	ϵ_s Spruce	ϵ_s Poplar
REV1	$32 \times 32 \times 63$	0.3272	0.4858
REV2	$64 \times 64 \times 127$	0.3049	0.4278
REV3	$96 \times 96 \times 191$	0.3275	0.3818
REV4	$128 \times 128 \times 255$	0.3139	0.3854
REV5	$160 \times 160 \times 319$	0.3236	0.3905
REV6	$192 \times 192 \times 383$	0.3183	0.3889

Table 1 records the results on the solid fraction of the two samples. It is observed that the first volumes are not representative in the case of poplar because they are too small. Also, the solid fraction occupies 32% within the whole space for spruce and 38% for poplar.

3.2 Convergence of the Thermal Conductivity

Table 2 depicts the results on the macroscopic thermal conductivity for spruce and poplar. They are listed following the orthotropic axes of the material and the REV size. Compared to the work [17], the values are quite similar, especially when the volume size is increasing. Indeed, we found that the predictive values are $\lambda_R^t = 0.11$ W/m.K, $\lambda_T^t = 0.11$ W/m.K and $\lambda_L^t = 0.16$ W/m.K for spruce. In the case of poplar, $\lambda_R^t = 0.14$ W/m.K, $\lambda_T^t = 0.12$ W/m.K and $\lambda_L^t = 0.2$ W/m.K. This confirms that the present approach preserves the property ranges. On the other hand, we checked that the obtained values are bounded in their physical ranges [21]. The larger (lower) bound corresponds to phases placed in parallel (series). It is also possible to dissociate the effect of the solid fraction from the thermal conductivity by introducing mixtures laws, see [17] for more details.

Table 2. Thermal conductivity for each species in terms of the REV size

Sample	λ^t (W/m.K)	REV1	REV2	REV3	REV4	REV5	REV6
Spruce	λ_R^t	0.1160	0.1115	0.1131	0.1133	0.1124	0.1109
	λ_T^t	0.1194	0.1045	0.1155	0.1119	0.1139	0.1122
	λ_L^t	0.1706	0.1641	0.1714	0.1691	0.1705	0.1680
Poplar	λ_R^t	0.1767	0.1580	0.1330	0.1402	0.1415	0.1425
	λ_T^t	0.1676	0.1333	0.1226	0.1158	0.1212	0.1186
	λ_L^t	0.2487	0.2216	0.1990	0.1999	0.2024	0.2020

3.3 Performance of the Numerical Method

We are interested in the efficiency of the proposed numerical method and its accuracy to predict the macroscopic thermal conductivity. This can be quantified by the performance of the solver. In Table 3, for each REV size, we display the required CPU time in minutes as well as the maximum of the errors, over the orthotropic directions, committed in the computation of λ^t . The latter was considered as the stopping criterion fixed to 2×10^{-2} in the previous works [16, 17]. More importantly, it is worth underling that the last test on the volume REV6 required exorbitant CPU time following the strategy of [17] whereas only few minutes are needed now to get same outcomes. The results approve that the current methodology is more accurate and very cheap. This renders it a good candidate to handle large volumes at different positions.

Table 3. CPU time in minutes and the maximum value of residuals

REV number	Spruce		Poplar	
	CPU time (mins)	Max residuals	CPU time (mins)	Max residuals
REV1	3.37×10^{-2}	4.42×10^{-4}	1.74×10^{-2}	4.56×10^{-4}
REV2	1.71×10^{-1}	1.10×10^{-3}	1.89×10^{-1}	1.19×10^{-3}
REV3	7.50×10^{-1}	3.59×10^{-4}	8.24×10^{-1}	4.15×10^{-5}
REV4	2.23	2.78×10^{-4}	2.50	3.02×10^{-4}
REV5	5.44	5.29×10^{-4}	5.48	1.23×10^{-4}
REV6	10.21	1.78×10^{-5}	10.55	7.33×10^{-5}

4 Conclusion

In this paper we made use of the homogenization and finite volume methods to compute the thermal conductivity of spruce and poplar species in their orthotropic directions. The samples are scanned with a lab X-ray nanotomograph to obtain the 3D morphology. The latter was treated using image processing tools to retrieve the distribution of the phases and to generate the mesh. These data become inputs of the computational algorithm. The stationary diffusion problem is solved directly without passing through the transient regime. The goal is to save the computational cost and to enable large-size mesh to be treated. Numerical evidences were reported to address the effect of the representative elementary volume (REV) on the macroscopic property.

In future contributions, we outlook to provide a deep comparison between the predictive approach and the experimental measurements for several wood species including more than two phases. This is for instance the case of materials including fibers and binders. Because the wood is highly anisotropic, another interesting avenue is to study the impact of the cell walls orientation on the macroscopic property.

Acknowledgments. Communauté urbaine du Grand Reims, Département de la Marne, Région Grand Est and European Union (FEDER Champagne-Ardenne 2014–2020) are acknowledged for their financial support to the Chair of Biotechnology of CentraleSupélec and the CEBB.

Nomenclature

K_i	Control volume
C_p	Heat capacity ($\text{J.kg}^{-1}.\text{K}^{-1}$)
L	Longitudinal direction
x_i	Mass center
R	Radial direction
REV	Representative elementary volume
T	Tangential direction
u	Temperature (K)

Greek Symbols

$\partial\Omega$	Boundary
σ_{ij}	Cell face
δ	Continuous variation
ρ	Density (kg.m^{-3})
Δ	Discrete variation
Ω	Domain
Γ	Mesh
ϵ_s	Solid fraction
λ	Thermal conductivity ($\text{W.m}^{-1}.\text{K}^{-1}$)
α	Thermal diffusivity, ($\text{m}^2.\text{s}^{-1}$)
τ_{ij}	Transmissibility

References

1. Wood handbook—wood as an engineering material. Forest Service, U.S. Department of Agriculture. Forest Products Laboratory, Madison, WI (2010)
2. Delgado, J.M.P.Q., Ramos, N.M.M., Barreira, E., de Freitas, V.P.: A critical review of hygrothermal models used in porous building materials. *J. Porous Media* **13**(3), 221–234 (2010)
3. Van Bellegem, M., Steeman, M., Willockx, A., Janssens, A., De Paepe, M.: Benchmark experiments for moisture transfer modelling in air and porous materials. *Build. Environ.* **46**(4), 884–898 (2011)
4. Woloszyn, M., Rode, C.: Tools for performance simulation of heat, air and moisture conditions of whole buildings. *Build. Simul.* **1**, 5–24. Springer (2008)
5. Hunt, J.F., Gu, H., Lebow, P.K.: Theoretical thermal conductivity equation for uniform density wood cells. *Wood Fiber Sci.* **40**, 167–180 (2008)
6. Brodersen, C.R.: Visualizing wood anatomy in three dimensions with high-resolution X-ray micro-tomography (μCT)—a review. *IAWA J.* **34**(4), 408–424 (2013)

7. Badel, É., Perré, P.: Predicting oak wood properties using X-ray inspection: representation, homogenisation and localisation. Part I: digital X-ray imaging and representation by finite elements. *Ann. For. Sci.* **59**(7), 767–776 (2002)
8. Baensch, F., et al.: Damage evolution in wood: synchrotron radiation micro-computed tomography (SR μ CT) as a complementary tool for interpreting acoustic emission (AE) behavior. *Holzforschung* **69**(8), 1015–1025 (2015)
9. Bucur, V.: *Nondestructive characterization and imaging of wood*. Springer Science and Business Media (2003)
10. Lux, J., Delisée, C., Thibault, X.: 3D characterization of wood based fibrous materials: an application. *Image Anal. Stereology* **25**(1), 25–35 (2006)
11. Standfest, G., Kranzer, S., Petutschnigg, A., Dunky, M.: Determination of the microstructure of an adhesive-bonded medium density fiberboard (MDF) using 3D sub-micrometer computer tomography. *J. Adhes. Sci. Technol.* **24**(8–10), 1501–1514 (2010)
12. Zauner, M., Stampanoni, M., Niemz, P.: Failure and failure mechanisms of wood during longitudinal compression monitored by synchrotron micro-computed tomography. *Holzforschung* **70**(2), 179–185 (2016)
13. Hunt, J.F., Gu, H.: Two-dimensional finite heat transfer model of softwood. Part I. Effective thermal conductivity. *Wood Fiber Sci.* **38**(4), 592–598 (2006)
14. Sova, D., Porojan, M., Bedelea, B., Humnic, G.: Effective thermal conductivity models applied to wood briquettes. *Int. J. Therm. Sci.* **124**, 1–12 (2018)
15. Perré, P., Turner, I.: Determination of the material property variations across the growth ring of softwood for use in a heterogeneous drying model. Part 2. Use of homogenisation to predict bound liquid diffusivity and thermal conductivity. *Holzforschung* **55**(4), 417–425 (2001)
16. Louërat, M., Ayouz, M., Perré, P.: Heat and moisture diffusion in spruce and wood panels computed from 3D morphologies using the Lattice Boltzmann method. *Int. J. Therm. Sci.* **130**, 471–483 (2018)
17. Quenjel, E.H., Perré, P.: Computation of the effective thermal conductivity from 3D real morphologies of wood. *Heat Mass Transf.* **58**, 2195–2206 (2022)
18. Otsu, N.: A threshold selection method from gray-level histograms. *IEEE Trans. Syst. Man Cybern.* **9**(1), 62–66 (1979)
19. Hornung, U.: Miscible displacement. In: *Homogenization and Porous Media*, pp. 129–146. Springer (1997)
20. Suquet, P. M.: Elements of homogenization for inelastic solid mechanics. In: *Homogenization Techniques for Composite Media*, vol. 272. Springer–Verlag (1985)
21. Siau, J.F.: *Transport processes in wood*. Springer-Verlag (1984)